Silicification of Peptide-Coated Silver Nanoparticles—A Biomimetic Soft Chemistry Approach toward Chiral Hybrid Core–Shell Materials

Philipp Graf,[†] Alexandre Mantion,[‡,*] Andrea Haase,[§] Andreas F. Thünemann,[‡] Admir Mašić,[⊥] Wolfgang Meier,[†] Andreas Luch,[§] and Andreas Taubert[⊥,¶,*]

[†]Department of Chemistry, Klingelbergstrasse 80, University of Basel, CH-4056 Basel, Switzerland, [‡]BAM Federal Institute for Materials Research and Testing, Richard-Willstaetter-Strasse 11, 12489 Berlin, Germany, [§]BfR—Federal Institute for Risk Assessment, Department of Product Safety, Thielallee 88-92, 14195 Berlin, Germany, [⊥]Max Planck Institute of Colloids and Interfaces, 14476 Golm, Germany, and [¶]Institute of Chemistry, University of Potsdam, 14476 Golm, Germany

ABSTRACT Silica and silver nanoparticles are relevant materials for new applications in optics, medicine, and analytical chemistry. We have previously reported the synthesis of pH responsive, peptide-templated, chiral silver nanoparticles. The current report shows that peptide-stabilized nanoparticles can easily be coated with a silica shell by exploiting the ability of the peptide coating to hydrolyze silica precursors such as TEOS or TMOS. The resulting silica layer protects the nanoparticles from chemical etching, allows their inclusion in other materials, and renders them biocompatible. Using electron and atomic force microscopy, we show that the silica shell thickness and the particle aggregation can be controlled simply by the reaction time. Small-angle X ray scattering confirms the Ag/peptide@silica core–shell structure. UV–vis and circular dichroism spectroscopy prove the conservation of the silver nanoparticle chirality upon silicification. Biological tests show that the biocompatibility in simple bacterial systems is significantly improved once a silica layer is deposited on the silver particles.

KEYWORDS: peptide-templated materials · silver nanoparticles · chiral nanoparticles · Ag/peptide@SiO_2 nanostructures · core–shell structures

Metal nanoparticles, especially silver nanoparticles, are important building blocks for sensors[1], medical[2–4] and optical devices.[5] Silver nanoparticles and composites are also found in an increasing number of end user consumer products (textiles, cosmetics, food contact material) because of their antibacterial properties. Metal nanoparticle synthesis is well established,[6–8] and more recent synthetic efforts are geared toward a better control over particle shape, size (distribution), or chirality. For many applications, metal nanoparticles need to be biocompatible or carry special functionalities. Among others, peptides have been used as efficient tools for controlling silver nanoparticle shape and size.[9–13] In some cases, elaborate scaffolds for the synthesis of complex silver nanoparticle/peptide hybrids have been made.[10] Overall, peptides combine good control over structure and chiral induction from the peptide to the metallic structure,[14,15] but also improve nanoparticle dispersibility and chemical stability.[9,16] This makes peptides attractive for nanoparticle protection and functionalization in a large variety of environments and for a number of inorganic nanoparticles.

Less noble metal nanoparticles such as silver and copper are far more reactive than their bulk counterparts.[17] They must thus be protected from chemical etching, metal ion leaching, oxidation, or coagulation. Protection can be achieved *via* a dense ligand shell (typically aliphatic thiols) or *via* coating with an inert material. Among others, silica has attracted interest as a nanoparticle coating material.[18] This is because silica is light compared to other inorganics, biocompatible, and chemically inert under most circumstances. Moreover, there are a series of protocols for further chemical modification of the silica shell. Colloidal,[19] optical,[20–22] and catalytic[23–25] properties of such hybrids can thus be tailored rather precisely, as has for example been shown for photonic crystals.[26–28]

Unfortunately, many nanoparticles are relatively difficult to coat with a silica layer of uniform thickness and density. Moreover, aggregation can often not be prevented, such that, in the end, relatively poorly defined metal nanoparticle/silica composites are obtained.[19] Different solutions have been developed, for example the coating of the metallic nanoparticles with a primary layer of silica precursor,[19,24,29–32] a biopolymer,[33] gelatin,[34] or coating of the particles

*Address correspondence to alexandre.mantion@bam.de, ataubert@uni-potsdam.de.

Received for review July 26, 2010 and accepted January 12, 2011.

Published online January 31, 2011
10.1021/nn102969p

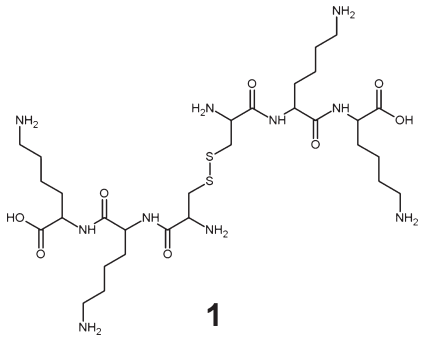

Scheme 1. Peptide 1 used for surface modification of the silver nanoparticles. The neutral form of the peptide is shown. The peptide sequence is CKK (single amino acid letter code). Two tripeptides are connected through a disulfide bridge (−S−S−). All amino acids are L-amino acids

with a silane-functionalized thiol followed by a Stöber process.[35] Alternatively, harsher conditions such as hydrothermal reactions or hydrolysis at higher temperatures have been proposed.[25,36]

A strategy not pursued much is the immobilization of catalytic units on the surface of the metal nanoparticles followed by the controlled hydrolysis of a silica precursor. This concept is based on the finding that basic peptides such as the silaffins[37,38] catalyze the hydrolysis of silica precursors like sodium silicate or tetraethylorthosilicate (TEOS) to form nanoscale silica. A similar process is also possible with synthetic polymers, leading to well-defined silica nanostars[39] or other shapes on patterned surfaces.[40−42] It should therefore be possible to exploit the catalytic activity of peptides and synthetic polymers to construct more complex nanoscale hybrid architectures. While there have been a few examples exploiting polymers and biopolymers for the synthesis of silica hybrid structures,[33,34,38,39,43−48] there have been no studies on the effect of particles coated with small tailor-made peptides as templates and catalysts for silicification.

The current study explores the possibility of using a well-defined peptide (Scheme 1) shell on the surface of a metal nanoparticle to control the growth of a very thin silica layer, whose thickness can be adjusted by selection of appropriate reaction parameters. A point of special interest is the formation of individual nanoparticles; that is, we were especially interested in suppressing the formation of aggregates of nanoparticles covered with one common silica shell or aggregates of Ag/SiO_2 particles without a predetermined order.

RESULTS

The peptide-modified silver nanoparticles have been described in a previous publication.[9] They can be dispersed in acidic aqueous solution as individual particles and aggregate at higher pH because of the deprotonation of the lysine residues and the resulting lower electrostatic repulsion. As shown by X-ray photoelectron spectroscopy (XPS),[9] the nanoparticles are coated almost exclusively by the peptide. The current study focuses on the silicification of these particles, where the peptide surface acts as a catalyst for TEOS hydrolysis. Because the peptide-catalyst is immobilized on the particle surface, the silicification is expected to only occur on the surface of the silver particles leading to well-defined Ag/peptide@SiO_2 nanoparticles.

Figure 1 shows representative transmission electron microscopy (TEM) images of the silica−silver hybrid materials after TEOS addition to a dispersion of the peptide-modified silver nanoparticles. The precursor nanoparticles are spherical with a radius of 10 nm and well-dispersed.[9] After one day of silicification, an additional layer appears on the silver particles. It can be attributed to a 2−4 nm thick silica shell. After 2 days, the particles are coated with a thicker shell of *ca.* 6−7 nm. While most particles are still present as individual particles, some aggregates are also observed after 2 days. After 3 days, larger aggregates (3−5 Ag/peptide@SiO_2 per aggregate) form, but some particles remain as individual Ag/peptide@SiO_2 nanoparticles. These samples also contain some silica without silver particles, indicating a less homogeneous process than during the first 2 days. After 4 days, there are only a few isolated particles present in solution. The large majority of the hybrid material is aggregated in large clusters containing more than 10 Ag/peptide@SiO_2 per aggregate. TEM therefore shows a well-controlled growth of the silica shell during the first two days of reaction. TEM also shows that the reaction time can be used to control the thickness of the growing amorphous silica. The control over the state of aggregation is less efficient once the reaction time is larger than *ca.* 2 days.

Figure 2 shows a high magnification scanning electron microscopy (SEM) image of the Ag/peptide@SiO_2 nanoparticles after 48 h of reaction time. Low magnification overview images show that the particles are spherical and relatively monodisperse with an average radius of *ca.* 15 nm. Aggregation is mostly a drying artifact. Closer inspection of the SEM images shows that there are two areas in the objects, an electron-dense core (Ag) and an electron-poor rim (SiO_2). SEM thus confirms TEM data, where also a core−shell architecture is observed. The shape at ambient conditions (that is, not under vacuum), and the shell growth upon silicification time was also studied by AFM, see Supporting Information, Figure S1 and S2. Essentially, AFM indicates that the objects are round, and the shell grows with time, identical to SEM and TEM data.

Figure 3 shows a representative energy dispersive X-ray (EDX) spectrum of the Ag/peptide@SiO_2 nanoparticles. All spectra clearly indicate the presence of silver, carbon, oxygen, nitrogen, and sulfur. This strongly supports the Ag/peptide@SiO_2 material structure in the sense that EDX detects silver from the original nanoparticle, nitrogen and sulfur from the peptide, and silicon from the shell. Oxygen and carbon are

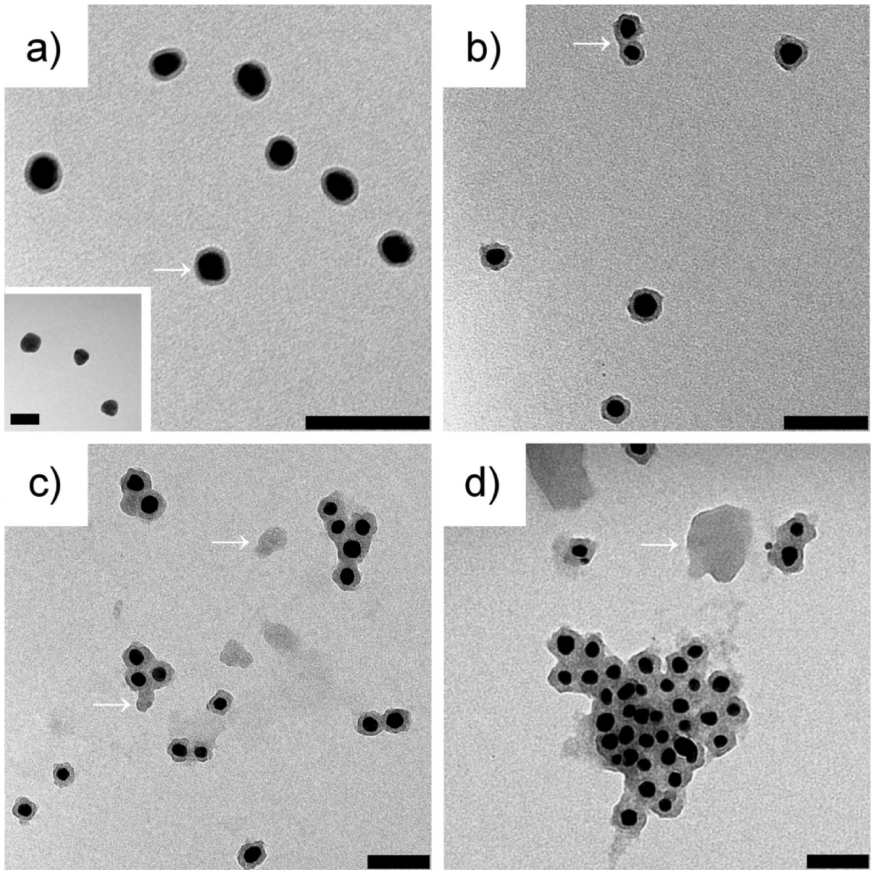

Figure 1. TEM images of Ag/peptide@SiO_2 (a) after 1 day, the arrow pointing to the growing silica shell, (b) after 2 days with the arrow indicating two aggregated particles, (c) after 3 days, the arrows pointing to empty silica material, and (d) after 4 days; the arrow points to a large silica particle without silver core. Scale bar is 100 nm in all images. Inset in panel a shows the particles before coating. Scale bar is 50 nm.

due to the peptide, possibly also some residual TEOS or ethoxy groups that have not reacted, and the sample support.

As microscopy is a very local technique, we have performed complementary small-angle X ray scattering (SAXS) measurements on the samples after silicification. Figure 4 shows the scattering curve of a dispersion of 1 mg/mL after 48 h of reaction. The SAXS pattern shows a minimum at around $q = 0.4$ nm^{-1} and a second minimum at around $q = 0.8$ nm^{-1}. The curve shows a Porod behavior where I(q) scales to q^{-4} for $q > 1$ nm^{-1}. This indicates a sharp interface of the nanoparticles with their surrounding. Both visible minima indicate a moderate polydispersity, which is surprising for a core−shell system. The increase in the low q region shows an attractive force between the particles. To avoid ambiguous curve fitting results, only the q region between 0.3 and 2 nm^{-1} was considered for shell thickness determination (assuming shell monodispersity and polydisperse core radius). The mean silver nanoparticle radius is 9.1 ± 0.2 nm, with a polydispersity of 17% and a shell thickness of 3.7 ± 0.2 nm. This is in acceptable agreement with experimentally determined values from TEM both in the current and the previous study.[9] To check our hypothesis, a second model was used, were the polydispersity is identical for both core and shell, but the ratio of the core radius to core radius + shell thickness is kept constant. This model leads to a worse curve fitting but leads to similar results, see Figure S4 (Supporting Information).

For a better insight into the nanoparticle structure, an experimental pair distribution function $P(r)$ evolution and its deconvolution were calculated from the experimental SAXS data in order to obtain an electron density function $\rho(r)$, Figure 5. $P(r)$ simulated from DECON and determined experimentally from the scattering curve by GIFT are in good agreement. $P(r)$ shows a behavior typical of a core−shell structure, as expected from TEM and SEM. More interestingly, the electron density curve $\rho(r)$ also shows that there are two types of electron density in the nano-object: an electron-rich core (the silver nanoparticle) and an electron-poor shell (the silica layer). The boundary between the two phases is located at around 10.5 nm, in fair agreement with the silver nanoparticle core radius determined by SAXS fitting and from TEM, Figure 1.

Furthermore, the electron density contrast between the surrounding medium and the nanoparticle is zero at around 15 nm, again suggesting that the whole

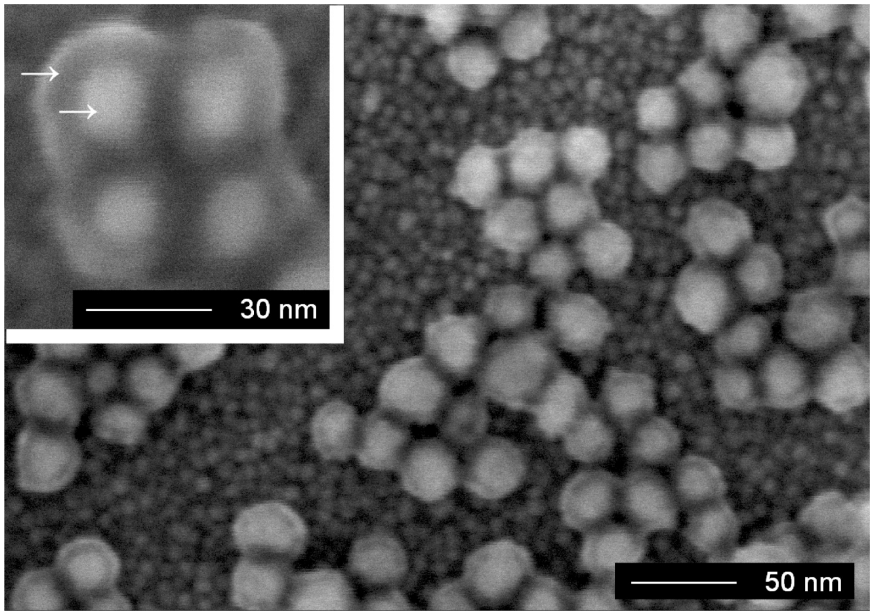

Figure 2. High magnification (300 000×) SEM image of the Ag/peptide@SiO_2 nanoparticles after 48 h of silicification. The small, *ca.* 4 nm, particles visible in the background are from the sample support and should not be confused with the silver nanoparticles (see Materials and Methods for details). Inset: Details of a nanoparticle aggregate. Arrows point to the silica shell (outside) and the silver core (inside). Note that the samples were not sputtered before imaging, and the contrast is due to the atomic number.

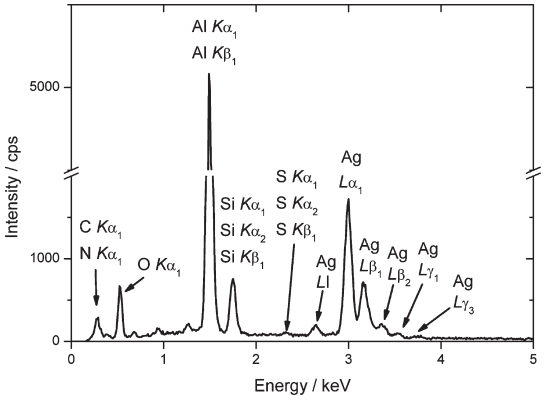

Figure 3. Energy-dispersive X ray spectrum from the nanoparticles presented in Figure 2 and peak assignments.[49] The aluminum signal arises from the sample holder.

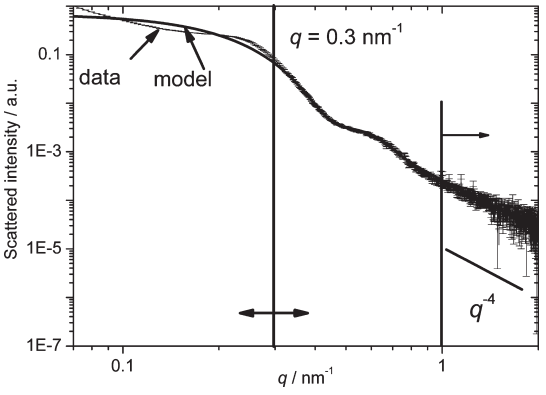

Figure 4. SAXS curve of Ag/peptide@SiO_2 nanoparticles (thin line) and a polydisperse core−shell model fitted to the data beyond q = 0.3 nm^{-1} (thick line). The Porod region is shown with a straight line. Curve fitting at high q is virtually undistinguishable from the experimental data.

hybrid nanoparticle has a radius on average of 15 nm, that is, the shell thickness is around 4.5 nm, which is in good agreement with TEM. In essence, SAXS correlates well with SEM and TEM, indicating that satisfactory assumptions were made in the SAXS data fitting model.

Metal nanoparticle shapes, their assembly, and dielectric environment can easily be determined using UV−vis spectroscopy.[5,50−52] Figure 6 shows the UV−vis spectra of peptide-coated silver nanoparticles and Ag/peptide@SiO_2 nanoparticles *versus* reaction time. For a better insight into the optical characteristics of the core−shell structures, a deconvolution similar to our previous publication was performed.[9] Table 1 summarizes the absorption maxima obtained from spectrum fitting *versus* reaction time. Peptide-coated nanoparticles exhibit maxima at 352, 376, 414, 442, and 497 nm, which are due to scattering and plasmon resonance of single nanoparticles.[51,52] The band at 497 nm indicates that some particles are distorted.[51] The bands at 600 nm are barely visible,[52] indicating that the particles are well dispersed in the medium.[9]

Upon addition of TEOS, the overall shape of the absorption curves remains unchanged. A small peak at 534 nm appears, likely caused by some aggregates. As the silica layer increases (Figure 1) there is a red-shift in the surface plasmon polariton resonance for the non-distorted and distorted nanoparticles (from 442 nm to *ca.* 459 nm and from 497 nm to *ca.* 530 nm, see Table 1). This is expected from Mie Theory,[53] even though not all bands are affected. This shift is due to the fact that the

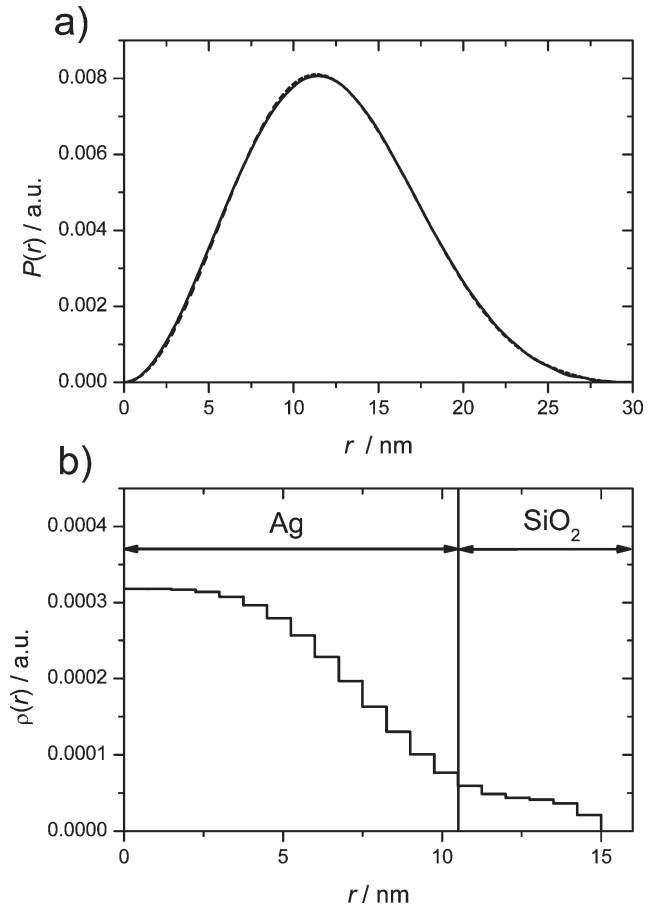

Figure 5. (a) Experimental pair distribution function *P*(*r*) as determined from the scattering curve *via* GIFT (dashed line) and the same curve obtained *via* DECON modeling (solid line). (b) Electronic density function $\rho(r)$ as calculated from the experimental *P*(*r*) function.

dielectric environment of the plasmon resonance changes from water to silica.[54,55] Interestingly, the plasmon resonance shift does not scale linearly with the silica layer thickness. This suggests that the silver nanoparticle is effectively shielded from the solvent after the silica layer has reached a certain thickness, and thus does not experience its dielectric influence anymore.

Finally, weak bands above 600 nm present in the samples prepared after 3 or 4 days are indicative of electronically coupled nanoparticles showing aggregation,[52] as confirmed by TEM.[9] Altogether, this indicates that particles coated with silica tend to aggregate but remain stable for short times, typically 1−2 days. UV-Vis thus demonstrates that even after 3 days the optical properties of the particles remain the same. This suggests that our particles could be interesting for the construction of optical devices.

Figure 7 shows IR spectra of the pure peptide, the peptide-coated silver nanoparticles, and the Ag/peptide@SiO_2 nanoparticles. The spectra of the peptide and the peptide-coated silver particles were described earlier and are only shown for comparison.[9] In short, the spectrum of the peptide-coated silver nanoparticles is controlled by the special selection rules of objects adsorbed on a metallic surface, thus leading to the apparently poor infrared spectrum. The infrared spectra of the Ag/peptide@SiO_2 nanoparticles shows intense signals arising from the amorphous silica layer, with broad bands at around 800, 950, 1044, and 1188 cm^{-1}. These bands can be attributed to ν(Si−O), δ(Si−OH), ν(Si−O−Si), and $\delta(CH_2)$ from residual TEOS or Si-ethoxy residuals from incomplete TEOS hydrolysis present at or included in the surface.[56,57] In strong contrast, the peptide signals are virtually invisible. In summary, IR spectroscopy supports the presence of an amorphous silica layer on the particle surface but does not show the presence of the peptide at the metal surface.

Raman spectroscopy at metal interfaces is a valuable method for the detection of small amounts of organic molecules and their orientation with respect to the metallic surface. This is similar to IR spectroscopy, but often Raman spectroscopy is more sensitive. Figure 8 shows complementary Raman spectra of Ag/peptide@SiO_2 and peptide-coated silver nanoparticles. As shown previously,[9] the peptide-coated nanoparticles show a complex spectrum with signals from carbonyl, amide, and aliphatic groups. Closer inspection of the Raman spectrum of the Ag/peptide@SiO_2 nanoparticles

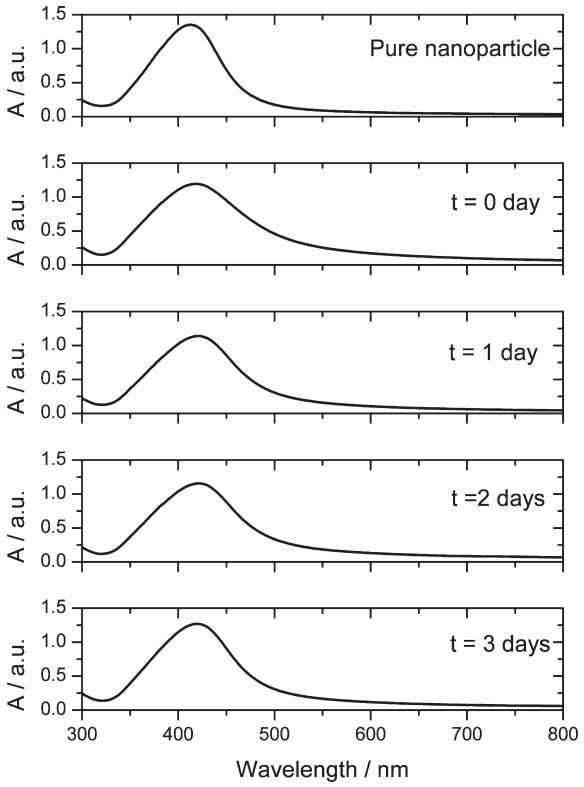

Figure 6. UV−vis spectra of the Ag/peptide@SiO_2 nanoparticles *versus* silicification time. Bands below 300 nm are due to the peptide coating. Particles were dispersed in bidistilled water at pH 3.

TABLE 1. UV−Visible Spectral Deconvolution[a]

sample	peak positions from deconvolution (nm)
pure particles	352 376 414 **442 497**
Day 1	354 377 414 **456 534**
Day 2	354 377 419 **460 526**
Day 3	354 377 418 **459 525** 643
Day 4	354 377 419 **458 522** 717

[a] Wavelengths of red-shifting peaks are bold. Peaks were modeled with Gaussian peaks. Representative deconvolution curves are shown in the Supporting Information (see Figure S5 and S6).

reveals the presence of additional bands at 460, 660, 817, and 1297 cm^{-1}. These correspond to γ(Si−O),[58,59] nonbridging oxygen atoms in silica and TEOS, δ(Si−O)[58−61] and ν(C−C) in TEOS.[62] Raman spectroscopy thus further confirms the presence of silica and some unreacted or partially reacted TEOS on the silver nanoparticles.

The fact that the two spectra shown in Figure 8 overlap almost perfectly (except for the count rates) indicates that there is no change at the nanoparticle surface, and thus the peptide is still present in its previous conformation. This finding cannot be inferred from IR spectroscopy but Raman spectroscopy confirms that the silicification *via* the lysine-based peptide **1** is a soft method, which conserves the organization of the peptide in the inorganic silica matrix.

Figure 9 shows the circular dichroism (CD) spectra of the Ag/peptide@SiO_2 and peptide-coated silver

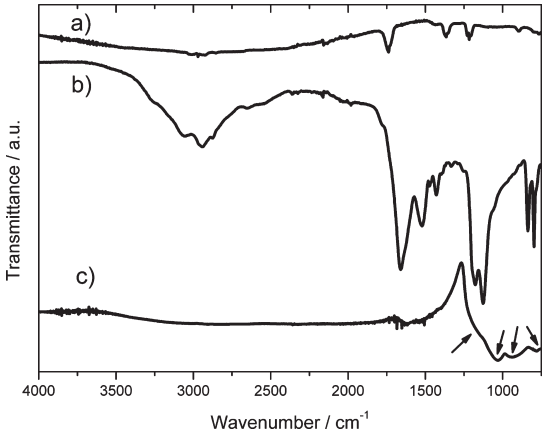

Figure 7. IR spectra of (a) the peptide-coated silver nanoparticles, (b) the neat peptide, and (c) the Ag/peptide@SiO_2 nanoparticles. Spectra where shifted vertically for clarity. Arrows point to the silica shell signals (see text for details).

nanoparticles. Both spectra show a chiral signature similar to gluthathione-protected silver clusters.[63] There are at least two Cotton points, one at around 300 nm common for both substances and a second one at 412 nm for Ag/peptide@SiO_2 and 377 nm for the peptide-coated silver nanoparticle. A simple explanation for the observed CD signal is difficult because of the many bands overlapping in this region (Supporting Information, Figure S7 and S8).

Nevertheless, the first Cotton point in the spectra of the peptide-modified nanoparticles can be attributed

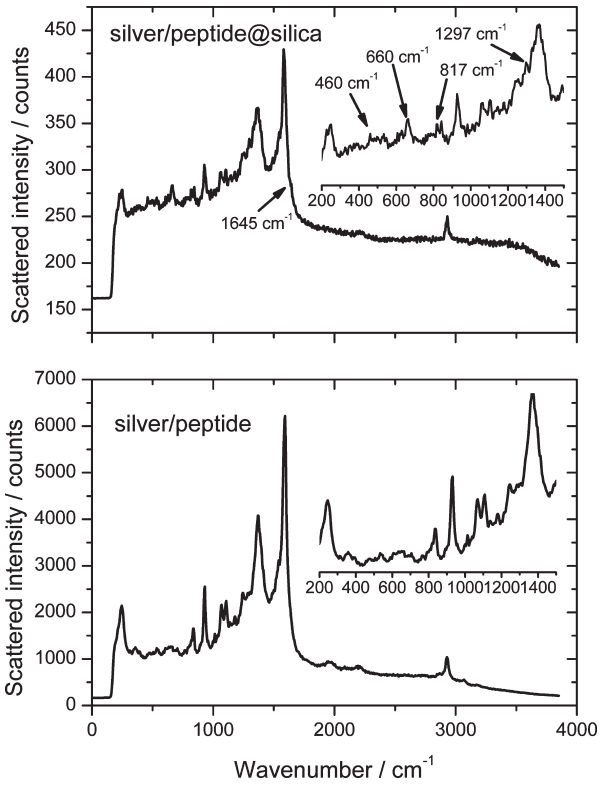

Figure 8. Raman spectra of Ag/peptide@SiO_2 (top) and peptide-coated silver nanoparticles (bottom). The inset shows an expanded view of the low frequency area, where the spectral signals of the inorganic components are located. The hump at 1645 cm^{-1} is caused by the carboxylate deprotonation at the peptide C terminus.

to the peptide, because of its low-lying frequency. However, a comparison with a CD spectrum taken from an aqueous solution of the pure peptide has been inconclusive, mainly because upon peptide adsorption onto the metallic surface, some additional interactions may be present and directly affect the CD signal.

The second Cotton point is presumably due to the plasmon resonance of the chiral silver nanoparticle. This is supported by previous modeling of chiral gold clusters[14] and experimental studies on chiral gold[14] and silver nanoparticles.[63−65] In these cases, the plasmon resonance presents a chiral signature, indicative of an asymmetric (chiral) atomic arrangement in the nanoparticle. Indeed, we have already reported[9] that the crystal structure of our nanoparticles is also chiral. However, a direct interpretation of the experimental plasmon band as a proof of intrinsic chirality is not straightforward. This is because possible Coulombic interactions between the plasmon from the metallic nanoparticle and the covalently linked peptide could also be the origin of this CD signal.[66] Further structural investigations of the nanoparticles to clarify these issues are underway.

Upon addition of the silica layer, the shape of the CD curve retains its general shape, but the plasmon bands red-shift by 37 nm (see UV−visible spectroscopy). This is consistent with literature data on other silicified nanoparticles.[53] The peptide bands are essentially unaffected

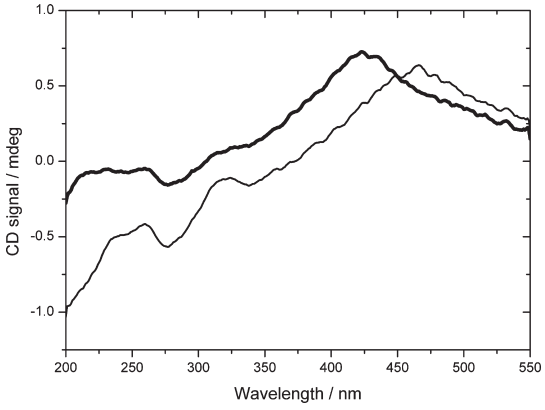

Figure 9. CD spectra of peptide-coated silver nanoparticles (bold line) and Ag/peptide@SiO_2 nanoparticles after 48 h of reaction (thin line). Absorbance was set to 1 at 420 nm. For a superposition with the respective deconvoluted UV−vis spectra, see Supporting Information, Figures S7 and S8.

by the silicification, which is in good agreement with Raman spectroscopy, evidencing that the peptide conserves its orientation on the nanoparticle surface.

As a result, CD spectroscopy clearly shows that 20 nm silver nanoparticles coated with a chiral peptide exhibit a CD signal. Although the origin of the CD signal can at the moment not unequivocally[66] be assigned, it is a clear demonstration that chiral core−shell organic−inorganic nanoparticles can be made and that the chiral information is conserved throughout the

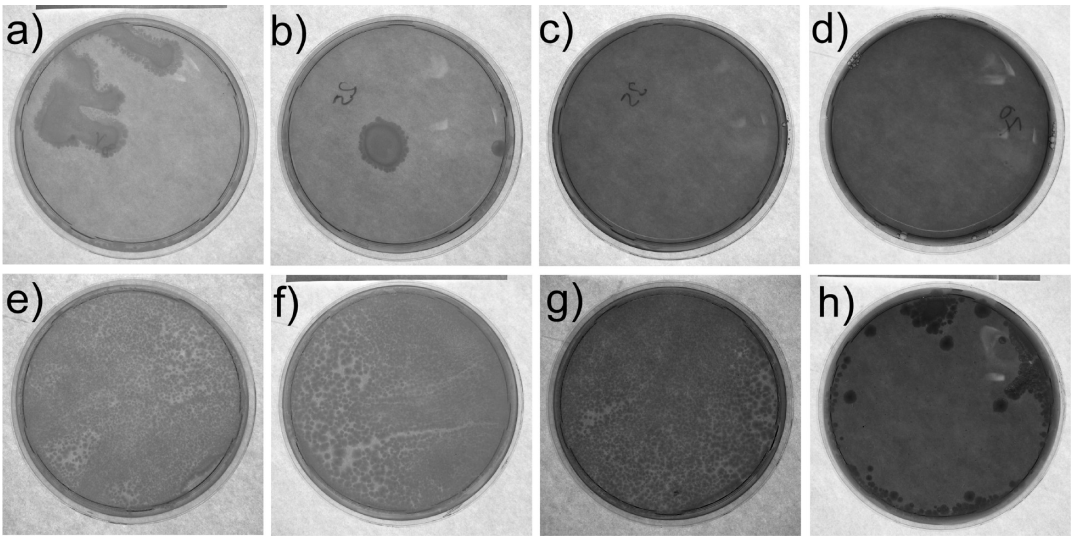

Figure 10. Photographs of Agar plates: (top row) peptide-coated silver nanoparticles, (bottom row) Ag/peptide@SiO_2 nanoparticles. Nanoparticle concentrations are in both cases (a, e) 18, (b, f) 25, (c, g) 35, and (d, h) 70 μg/mL. Bacteria concentration: 5×10^5 CFU. Incubation time is 24 h at 37 °C.

entire process. The data therefore show, unlike earlier, more ambiguous accounts,[65,67] that chirality in complex hybrid nanoparticles can successfully be conserved and encoded.

Silver nanoparticles are often studied for their antibiotic properties.[68] Sometimes these highly desirable properties may, however, hamper further use, for example in confocal Raman spectroscopy *in vitro* or even *in vivo*. As a result, we have studied the effect of our nanoparticles on *E. coli* K12 to evaluate if the silica coating could be used as a protective shell against antibiotic activity while keeping the useful optical properties.

Figure 10 shows photographs of modified diffusion experiments after 24 h for both peptide-coated nanoparticles and Ag/peptide@SiO_2 nanoparticles in a concentration range between 18 and 70 μg/mL. For the peptide-coated nanoparticles, a minimal bacteriostatic concentration of 35 micrograms/mL was determined, similar to results in comparable conditions.[69−71] In contrast, bacterial growth in the presence of Ag/peptide@SiO_2 is not affected by the presence of the particles. At higher nanoparticle concentration the growth is likely to be slowed down, but not stopped. In this case the particles have a nonspecific toxicity, as usually found for nanoparticles at a concentration above *ca.* 100 μg/mL.

A 10-fold increase of the bacterial concentration (Figure 11) leads to a doubling of the minimal inhibitory concentration to more than 100 μg/mL. Such a tendency has already been reported.[69,71] Again, however, there is no growth perturbation in the case of the Ag/peptide@SiO_2 nanoparticles, as the bacteria layer density is in all cases similar.

In conclusion, these results suggest that the Ag/peptide@SiO_2 nanoparticles are (relatively) safe for living systems and can probably be used for imaging purposes. Not surprisingly, the peptide-coated silver nanoparticles (without the silica coating) exhibit antibacterial properties similar to other systems already investigated.

To further investigate the potential of the nanoparticles as sensors in more complex living systems, human cell type were used for further investigation. Figure 12 shows results of viability tests of macrophages differentiated from THP-1 cells after 24 and 48 h of incubation with Ag/peptide@SiO_2, peptide-coated silver, and peptide-coated gold nanoparticles. Viabilities after 24 and 48 h are similar. The peptide-coated gold nanoparticles are nontoxic up to a concentration of 50 μg/mL. In contrast, peptide-coated silver nanoparticles and Ag/peptide@SiO_2 affect the viability already at 10 μg/mL and lead to a complete human-type cell death at concentrations higher than 50 μg/mL for Ag/peptide@SiO_2. This is rather surprising, as it seems contradictory with the previous experiment involving bacteria. A close inspection of the cells incubated with 50 μg/mL shows that they are coated with a film of Ag/peptide@SiO_2, which can be attributed to the colloidal instability of silica nanoparticles in biological media, as for example plasma proteins are known to adsorb on silica surface and cause flocculation.[72−74] That is, the nanoparticles sediment on the cells and kill them by mechanical destabilization or by exposing them to (locally) very high nanoparticle concentrations, a point discussed earlier.[75] However, if concentrations below 10 μg/mL are considered, Ag/peptide@SiO_2 is well tolerated by the human cells, similar to peptide-coated silver and gold nanoparticles, but with a broader flexibility of the surface chemistry. Altogether, this preliminary study shows that Ag/peptide@SiO_2 nanoparticles are interesting but not yet optimal for biological studies. Further functionalization may alleviate this issue.

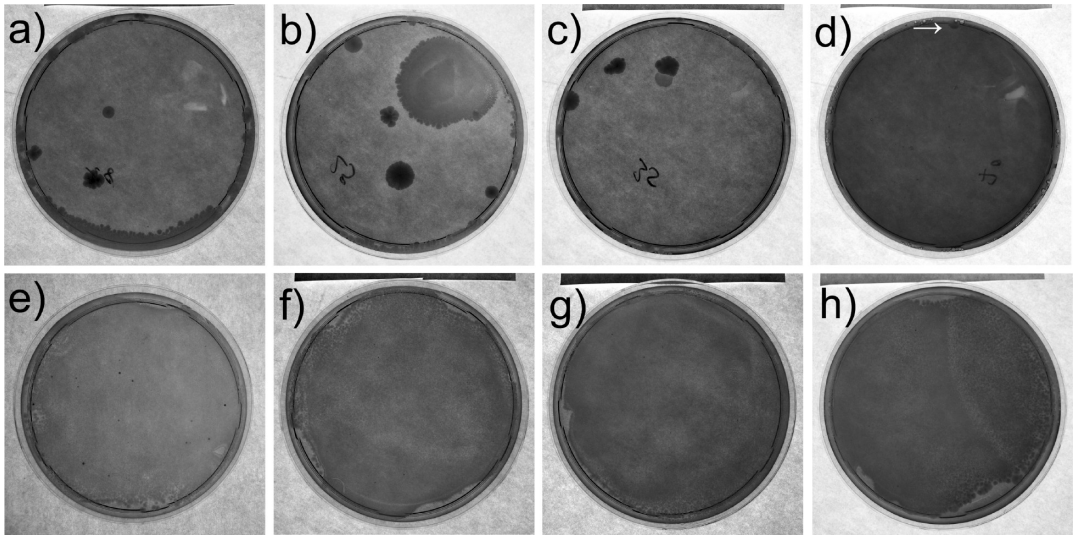

Figure 11. Photographs of Agar plates: (top row) peptide-coated silver nanoparticles, (bottom row) Ag/peptide@SiO_2 nanoparticles. Nanoparticle concentrations are in both cases (a, e) 18, (b, f) 25, (c, g) 35, and (d, h) 70 μg/mL. Bacteria concentration: 5×10^6 CFU (10$\times$ higher than in Figure 10). Incubation time is 24 h at 37 °C.

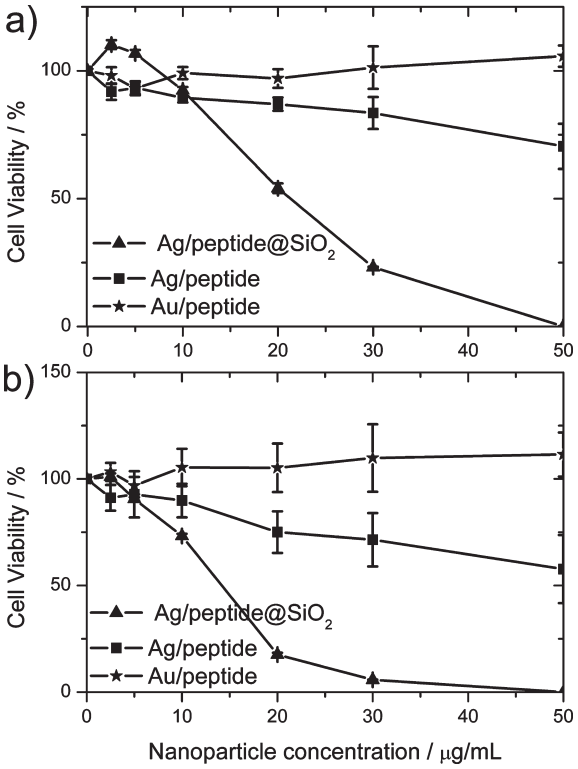

Figure 12. Viability assay of macrophages differentiated from THP-1 exposed for (a) 24 and (b) 48 h to Ag/peptide@SiO_2 (triangle), peptide-coated silver (square), and peptide-coated gold (star) nanoparticles.

DISCUSSION

One of the advantages of the synthetic protocol presented here is its simplicity and efficiency. The peptide acts as both a stabilizer and a silicification catalyst. That is, the nanoparticle surface is never exposed to the reaction medium and thus less prone to oxidation and to chemical etching. Further on, there is no need to first activate the nanoparticle surface, for example, with aminosilanes[19] or polymers,[33,34,76] before inducing a silica shell formation. Sol−gel processes, similar to the Stöber method have been proposed to form a silica shell around nanoparticles.[24,29−32,77] However, these processes can lead to the degradation of the ligand shell and, for example, to a loss of optical properties that are associated with both the chemistry and size of the nanoparticle and the organic shell. Similarly, if the silicification is done at higher temperatures,[78] the nanoparticles are more prone to aggregation. This

then causes problems with colloidal stability and reproducibility, for example, of their optical properties and generates batch-to-batch variations.

In essence, the methodology presented here is interesting because it takes advantage of the intrinsic ability of the lysine peptides to hydrolyze TEOS or similar silica precursors. The reaction can, unlike the examples just discussed, be performed at ambient conditions. Moreover, the fact that the peptide is, unlike some polymeric additives, well-defined and always has the same molecular weight, *etc.*, lends the process to automatic synthesis, which could be interesting for combinatorial approaches or parallel production of larger amounts of nanoparticles.

Moreover, the nanoparticles can further be functionalized using conventional silica modification chemistry, but, more interestingly, they also maintain their chiral information once the peptide is encapsulated in the silica matrix. Chiral nanoparticles are very interesting both for fundamental and applied questions.[79−81] There are different ways to prepare them; especially, noble metal nanoparticles can be prepared *via* the use of chiral ligands during the synthesis process.[14,15,79] The advantage of the current approach however is that their chiral information can be "protected" by way of the silica shell. Even subtle changes in the crystal structure[9] are conserved. The resulting nanoparticles are thus interesting building blocks for the creation of chiral metamaterials and other constructs that are currently investigated for their optical or magneto-optical properties.[54,82,83,26]

Finally, in light of the result from the biological tests (Figures 10−12), the particles presented here could be useful in a variety of ways. For example, upon adequate functionalization with proteins,[84] these particles could be used *in vivo* for imaging and localization thanks to their (optically active) Raman properties. Silver nanoparticles are also interesting for conveying antibiotic properties to implants, for example hydroxyapatite,[68,85,86] titania,[87] hydroxyapatite-zirconia,[88] and more complex bioglasses,[89] in particular for longer term delivery.[90,91] Overall, the process reported here is a simple, straightforward synthetic approach yielding a nanoscale, biomimetic coating on nanoparticles. It is useful for the synthesis and modification of a large number of nanoscale materials including biomaterials and optical components.

CONCLUSION

Peptide-coated silver nanoparticles can be easily coated with a silica shell of controllable thickness of as little as 1−2 nm using a biomimetic process operating at ambient conditions. The resulting particles exhibit better chemical stability and biological compatibility when compared to conventional silver nanoparticles. Moreover, the chiral information carried by the silver nanoparticle is also present after growth of the silica shell, implying that the nanoparticles could become of use for optical devices or sensing applications. This is particularly interesting, because the silica-coated nanoparticles are not toxic to *E. coli* and only show a limited toxicity toward THP-1 differentiated macrophages.

MATERIALS AND METHODS

General. Chemicals were obtained from Bachem (Bubendorf, Switzerland) or Fluka (Buchs, Switzerland) and used without further purification. All amino-acids are L-amino acids.

Silver Nanoparticle Preparation. Peptide **1** and silver nanoparticles were prepared as published,[9] and directly used after preparation, without freeze-drying but purified by repeated centrifugations. The preparation pH for the nanoparticle was 3.

Silicification. To a 1 mg/mL peptide-coated silver nanoparticle solution (20 mL, pH 3, ice cooled) 400 μL of ice-cooled tetraethoxysilane were added under strong stirring in a Teflon flask. After 1, 2, 3, and 4 days at 25 °C under vigorous stirring, samples were isolated and purified by repeated centrifugation/dispersion in water.

Transmission Electron Microscopy. TEM images were taken on an FEI Morgani 268D operated at 80 kV. Samples were deposited on carbon-coated copper grids and directly imaged after drying in air. Some samples were diluted prior to imaging to allow for better imaging conditions.

High Resolution Scanning Electron Microscopy (SEM). SEM images were taken on a Hitachi S-4800 with a field emission source at 5 kV, in secondary electron mode. Samples were measured without sputtering. Substrates were glass coverslips coated with platinum (4 nm) in a BalTec MED 020. For EDX, concentrated suspensions were directly deposited on an aluminum plate and larger aggregates were analyzed.

Thermogravimetric Analysis. TGA was performed with a Mettler Toledo TGA/SDTA 851e from 25 to 800 °C with a heating rate of 10 °C min^{-1} in N_2.

Infrared Spectroscopy. IR spectra were obtained from the neat samples on a Shimadzu FTIR 8300 with a Golden Gate ATR unit. Spectra were recorded from 300 to 4500 cm^{-1} with a resolution of 1 cm^{-1}. To ensure a good signal-to-noise ratio in the case of Ag/peptide@SiO_2 and peptide-coated nanoparticles, measurements were repeated 128 times.

Small-Angle X-ray Scattering. SAXS measurements were performed with a SAXSess camera (Anton Paar, Austria) attached to a laboratory X-ray generator (PW3830, PANanalytical) operated with a fine focus glass X-ray tube at 40 kV and 50 mA (Cu $K\alpha$, λ = 0.1542 nm). Samples were filled in a reusable vacuum tight 1 mm quartz capillary to attain the same scattering volume and background contribution. The scattering vector is defined in terms of the scattering angle θ, and the wavelength of the radiation thus $q = 4\pi/\lambda \sin(\theta)$. SAXS data were recorded as 700 × 1.2 s repetitions in a q-range of 0.04−5.0 nm^{-1} with a CCD detection system (Anton Paar). The two-dimensional intensity data were converted to one-dimensional data and deconvoluted using the software SAXSQuant (Anton Paar). Data were fitted using a model where the shell thickness is considered constant and the core radius polydisperse[92] assuming a Schultz distribution[93,94] of the radii, using Igor Pro 6.0.4 (Wavemetrics) and the SANS Data Analysis Package[95] (NIST). A second model was used to fit the data, this time assuming a constant shell/core + shell ratio,[96] and a Schultz distribution[93,94] of the radii (see Supporting Information for more details). Pair distribution functions were determined using a spherical symmetry using GIFT.[97] The program

DECON[98] was used to determine the radial electron density distribution $\rho(r)$.

UV−Visible Spectroscopy. Samples were measured in 1 cm quartz cuvettes on a Perkin-Elmer Lambda 25. Data were deconvoluted using Fytik.

Surface-Enhanced Raman Spectroscopy (SERS). Silver nanoparticles were investigated as dispersion in water with a confocal Raman microscope (CRM300, WITec, Germany) equipped with a piezo-scanner (P-500, Physik Instrumente, Germany), a 60× objective, and a 532 nm Nd:YAG laser. Spectra were acquired with an air-cooled CCD detector (DU401-BV, Andor, UK) with 600 gratings/mm (UHTS 300, WITec, Germany). ScanCtrlSpectroscopyPlus (version 2.04, WITec) was used for data acquisition and processing. Power was adjusted to have a good signal-to-noise ratio and to avoid sample destruction. Typically, less than 1 mW full beam power at the sample was applied. Samples were acquired as 100 repetitions of 1 s to ensure a good signal/noise ratio.

CD Spectroscopy. CD spectra were recorded on a Chirascan CD spectrophotometer (Applied Physics, United Kingdom). Samples were dispersed in aqueous HCl at pH 3 and experiments were done in 1 cm quartz cells. Absorbance was set to 1 au at 420 nm, scan rate was 5 s per nm, and resolution was 1 nm. Spectra were averaged and smoothed from 5 measurements between 200 and 550 nm.

Atomic Force Microscopy. Tapping mode AFM was done on a Molecular Imaging PicoLE system with a Super Sharp Silicon SFM-Sensor (SSS-NCHR-10, Nanosensor) with a tip radius of 2 nm, spring constant of 10−130 N m^{-1} and a resonance frequency of 204−497 kHz (values given by the manufacturer) or a Topometrix Explorer. Images were treated using Gwyddion. Samples were strongly diluted in ultrapure water (pH 3), spin-cast on a freshly cleaved mica wafer, and dried in air before imaging.

Biological Tests with *E. coli* K12. The bactericidal effect of both types of nanoparticles were investigated using LB agar plates supplemented with peptide-coated and Ag/peptide@SiO_2 nanoparticles to have a final concentration of 18, 25, 35, and 70 μg/mL of nanoparticles in the agar plate. To these were inoculated 100 μL of a 5×10^6 and 5×10^7 CFU solution of *E. coli* strain K12. The plates were cultured for 24 h at 37 °C. Test plates (without nanoparticles) showed a dense film of bacteria, see Supporting Information Figure S9. Experiments using peptide-coated 20 nm gold nanoparticles prepared from citrate-coated gold nanoparticles *via* ligand exchange with peptide **1** do not exhibit toxic properties for *E. coli* K12 until a concentration of 35 μg/mL and a concentration 10^5 CFU (see Supporting Information Figure S10 for more details).

Biological Tests with a Human Cells Line. THP-1 cell line was obtained from the Deutsche Sammlung für Mikroorganismen and Zellkulturen GmbH (DSMZ) stock collection. Cells were grown at 37 °C with 5% CO_2 in RPMI medium supplemented with 10% fetal calf serum, 2 mM L-glutamine, 10 mM HEPES, 1 mM pyruvate, 100 U/mL penicillin, and 0.1 mg/mL streptomycine. The differentiation into macrophage cell-like cells was performed by adding 100 ng/mL phorbol-12-myristate-13 acetate as described in the literature.[99,100] Cell viability after nanoparticle treatment was determined using WST-1 assay (Roche Applied Biosystem) according to the manufacturer instruction with modifications to make the assay applicable for nanoparticle treated cells. Briefly, cells were seeded in a 96-wells plate with a density of 1×10^4 cells per well, differentiated, and incubated with nanoparticles (4 replicates per concentration, 3 independent biological repeats). After 24 or 48 h, WST-1 reagent was added to the cells; the resulting solution was centrifuged to remove the physically interfering nanoparticles and spectrophotometric evaluation was performed. The relative viability (% viability in respect to control untreated cells) was calculated and expressed as a mean value and standard error of the mean (SEM) as a result of at least 3 independent biological measurements.

Acknowledgment. We thank an unknown reviewer for a very useful comment, Prof. E.C. Constable for access to his TGA and FT-IR, the Department of Chemistry (Basel) for access to the CD spectrometer, Dr. H.-J. Kunte for the *E. coli* K12 strain, V. Thommen-Geiser and T. Schuster for help with the AFM, D. De Bruyn for help with CD measurements, and M. Düggelin for help with the SEM. A. Mantion thanks the Adolf-Martens e.V. for an Adolf-Martens Fellowship. A. Mašić is grateful for support by the Alexander von Humboldt Foundation and the Max Planck Society in the framework of the Max Planck Research Award by the Federal Ministry of Education and Research. The Swiss National Science Foundation, the University of Potsdam, the Fonds der Chemischen Industrie, the Bundesanstalt für Materialforschung und -prüfung, the Bundesinstitut für Risikobewertung, and the MPI of Colloids and Interfaces (Colloid Chemistry Department) are thanked for financial support.

Supporting Information Available: Figure S1: Height profiles extracted from a Ag/peptide@SiO_2 nanoparticle monolayer after 2 days of reaction. Figure S2: AFM images of peptide-coated silver nanoparticles, Ag/peptide@SiO_2 nanoparticles after 24 and 48 h. Figure S3: Thermogravimetric investigation of the nanoparticles before and after 48 h silicification. Figure S4: SAXS curve fitting using a shell/core+shell radii ratio kept constant. Figure S5: Deconvolution of the UV−vis spectra from the silver nanoparticle solution. Figure S6: Deconvolution of the UV−vis spectra from a Ag@SiO_2 nanoparticle solution. Figure S7: CD spectra and the UV−vis spectra deconvoluted from the peptide-coated silver nanoparticles. Figure S8: CD spectra and the UV−vis spectra deconvoluted from the Ag/peptide@SiO_2 nanoparticles Figure S9: Photograph of a control agar plate without any nanoparticle. Figure S10: Control experiment with peptide-coated gold nanoparticles. This material is available free of charge *via* the Internet at http://pubs.acs.org.

REFERENCES AND NOTES

1. Lee, K. S.; El-Sayed, M. A. Gold and Silver Nanoparticles in Sensing and Imaging: Sensitivity of Plasmon Response to Size, Shape, and Metal Composition. *J. Phys. Chem. B* **2006,** *110*, 19220–19225.
2. Kvitek, L.; Vanickova, M.; Panacek, A.; Soukupova, J.; Dittrich, M.; Valentova, E.; Prucek, R.; Bancirova, M.; Milde, D.; Zboril, R. Initial Study on the Toxicity of Silver Nanoparticles (NPs) against *Paramecium caudatum*. *J. Phys. Chem. C* **2009,** *113*, 4296–4300.
3. Kang, M.; Jung, R.; Kim, H. S.; Youk, J. H.; Jin, H. J. Silver Nanoparticles Incorporated Electrospun Silk Fibers. *J. Nanosci. Nanotechnol.* **2007,** *7*, 3888–3891.
4. Chen, X.; Schluesener, H. J. Nanosilver: A Nanoproduct in Medical Application. *Toxicol. Lett.* **2008,** *176*, 1–12.
5. Evanoff, D. D.; Chumanov, G. Synthesis and Optical Properties of Silver Nanoparticles and Arrays. *ChemPhysChem* **2005,** *6*, 1221–1231.
6. Henglein, A.; Giersig, M. Formation of Colloidal Silver Nanoparticles: Capping Action of Citrate. *J. Phys. Chem. B* **1999,** *103*, 9533–9539.
7. Dahl, J. A.; Maddux, B. L. S.; Hutchison, J. E. Toward Greener Nanosynthesis. *Chem. Rev. (Washington, DC, U. S.)* **2007,** *107*, 2228–2269.
8. Daniel, M. C.; Astruc, D. Gold Nanoparticles: Assembly, Supramolecular Chemistry, Quantum-Size-Related Properties, and Applications toward Biology, Catalysis, and Nanotechnology. *Chem. Rev. (Washington, DC, U. S.)* **2004,** *104*, 293–346.
9. Graf, P.; Mantion, A.; Foelske, A.; Shkilnyy, A.; Masic, A.; Thuenemann, A. F.; Taubert, A. Peptide-Coated Silver Nanoparticles: Synthesis, Surface Chemistry, and PH-Triggered, Reversible Assembly into Particle Assemblies. *Chem.—Eur. J.* **2009,** *15*, 5831–5844.
10. Mantion, A.; Guex, A. G.; Foelske, A.; Mirolo, L.; Fromm, K. M.; Painsi, M.; Taubert, A. Silver Nanoparticle Engineering *via* Oligovaline Organogels. *Soft Matter* **2008,** *4*, 606–617.
11. Mantion, A.; Massuger, L.; Rabu, P.; Palivan, C.; McCusker, L. B.; Taubert, A. Metal−Peptide Frameworks (MPFs): "Bioinspired" Metal Organic Frameworks. *J. Am. Chem. Soc.* **2008,** *130*, 2517–2526.
12. Mantion, A.; Taubert, A. TiO_2 Sphere−Tube−Fiber Transition Induced by Oligovaline Concentration Variation. *Macromol. Biosci.* **2007,** *7*, 208–217.

13. Dickerson, M. B.; Sandhage, K. H.; Naik, R. R. Protein- and Peptide-Directed Syntheses of Inorganic Materials. *Chem. Rev. (Washington, DC, U. S.)* **2008,** *108*, 4935–4978.
14. Gautier, C.; Burgi, T. Chiral *N*-Isobutyryl-Cysteine Protected Gold Nanoparticles: Preparation, Size Selection, and Optical Activity in the UV−vis and Infrared. *J. Am. Chem. Soc.* **2006,** *128*, 11079–11087.
15. Gautier, C.; Burgi, T. Chiral Inversion of Gold Nanoparticles. *J. Am. Chem. Soc.* **2008,** *130*, 7077–7084.
16. Levy, R.; Thanh, N. T. K.; Doty, R. C.; Hussain, I.; Nichols, R. J.; Schiffrin, D. J.; Brust, M.; Fernig, D. G. Rational and Combinatorial Design of Peptide Capping Ligands for Gold Nanoparticles. *J. Am. Chem. Soc.* **2004,** *126*, 10076–10084.
17. Bertolini, J. C.; Rousset, J. L. Reactivity of Metal Nanoparticles. *Nanomaterials and Nanochemistry*; Springer: Berlin, 2008; pp 281304
18. Liu, S.; Han, M.-Y. Silica-Coated Metal Nanoparticles. *Chem.—Asian J.* **2010,** *5*, 36–45.
19. LizMarzan, L. M.; Giersig, M.; Mulvaney, P. Synthesis of Nanosized Gold−Silica Core−Shell Particles. *Langmuir* **1996,** *12*, 4329–4335.
20. Renteria-Tapia, V. M.; Valverde-Aguilar, G.; Garcia-Macedo, J. A. Synthesis, Optical Properties, and Modeling of Silver Core−Silver Oxide Shell Nanostructures in Silica Films. *Plasmon.: Metall. Nanostruct. Their Opt. Prop. V* **2007,** *6641*, W6411–W6411 (568).
21. Sun, X. F.; Wei, C. P.; Li, Q. Y.; Xu, J. Ag/SiO_2 Composite Thin Films: Preparation by UV Radiation Deoxidation and Optical Properties. *Chin. J. Inorg. Chem.* **2008,** *24*, 1895–1899.
22. Tanahashi, I.; Yoshida, M.; Manabe, Y.; Tohda, T.; Sasaki, S.; Tokizaki, T.; Nakamura, A. Preparation and Nonlinear-Optical Properties of Ag/SiO_2 Glass Composite Thin-Films. *Jpn. J. Appl. Phys., Part 2 Lett.* **1994,** *33*, L1410–L1412.
23. Ung, T.; Liz-Marzan, L. M.; Mulvaney, P. Redox Catalysis Using Ag@SiO_2 Colloids. *J. Phys. Chem. B* **1999,** *103*, 6770–6773.
24. Badr, Y.; Mahmoud, M. A. Photocatalytic Degradation of Methyl Orange by Gold Silver Nano-Core/Silica Nano-Shell. *J. Phys. Chem. Solids* **2006,** *68*, 413–419.
25. Lambert, S.; Cellier, C.; Gaigneaux, E. M.; Pirard, J. P.; Heinrichs, B. Ag/SiO_2, Cu/SiO_2 and Pd/SiO_2 Cogelled Xerogel Catalysts for Benzene Combustion: Relationships between Operating Synthesis Variables and Catalytic Activity. *Catal. Commun.* **2007,** *8*, 1244–1248.
26. Lee, H. B.; Yoo, Y. M.; Han, Y. H. Characteristic Optical Properties and Synthesis of Gold−Silica Core−Shell Colloids. *Scr. Mater.* **2006,** *55*, 1127–1129.
27. Lu, Y.; Yin, Y. D.; Xia, Y. N. Photonic Crystals Fabricated from Gold−Silica Core−Shell Nanoparticles. *Nanoscale Opt. Appl.* **2002,** *4809*, 197–201.
28. Ye, J.; de Broek, B. V.; De Palma, R.; Libaers, W.; Clays, K.; Van Roy, W.; Borghs, G.; Maes, G. Surface Morphology Changes on Silica-Coated Gold Colloids. *Colloids Surf. A* **2008,** *322*, 225–233.
29. Aslan, K.; Wu, M.; Lakowicz, J. R.; Geddes, C. D., Fluorescent Core−Shell Ag@SiO_2 Nanocomposites for Metal-Enhanced Fluorescence and Single Nanoparticle Sensing Platforms. *J. Am. Chem. Soc.* 2007, *129*, 1524.
30. Aslan, K.; Wu, M.; Lakowicz, J. R.; Geddes, C. D. Metal Enhanced Fluorescence Solution-Based Sensing Platform 2: Fluorescent Core−Shell Ag@Sio2 Nanoballs. *J. Fluoresc.* **2007,** *17*, 127–131.
31. Li, T.; Moon, J.; Morrone, A. A.; Mecholsky, J. J.; Talham, D. R.; Adair, J. H. Preparation of Ag/SiO_2 Nanosize Composites by a Reverse Micelle and Sol−Gel Technique. *Langmuir* **1999,** *15*, 4328–4334.
32. Xu, J.; Dong, J. F.; Nie, Q. H. Preparation and Optical Absorption of Ag/SiO_2 Core−Shell Spheres. *Rare Metal Mater. Eng.* **2008,** *37*, 277–280.
33. Chou, K. S.; Chen, C. C. Fabrication and Characterization of Silver Core and Porous Silica Shell Nanocomposite Particles. *Microporous Mesoporous Mater.* **2007,** *98*, 208–213.
34. Liu, S.; Zhang, Z.; Han, M.-Y. Nanometer-Sized Gold-Loaded Gelatin/Silica Nanocapsules. *Adv. Mater. (Weinheim, Ger.)* **2005,** *17*, 1862–1866.
35. Ming, M.; Chen, Y.; Katz, A. Synthesis and Characterization of Gold−Silica Nanoparticles Incorporating a Mercaptosilane Core−Shell Interface. *Langmuir* **2002,** *18*, 8566–8572.
36. Huang, C. J.; Chiu, P. H.; Wang, Y. H., Synthesis of Core@Shell Composites with Gold Nanoparticles Trapped inside Ceramic Silica Shells by the Sol−Gel Method. *Key Eng. Mater.* 2008, *368−372*, 797−799.
37. Kroger, N.; Deutzmann, R.; Sumper, M. Polycationic Peptides from Diatom Biosilica That Direct Silica Nanosphere Formation. *Science* **1999,** *286*, 1129–1132.
38. Sumper, M.; Kroger, N. Silica Formation in Diatoms: The Function of Long-Chain Polyamines and Silaffins. *J. Mater. Chem.* **2004,** *14*, 2059–2065.
39. Kind, L.; Plamper, F. A.; Gobel, R.; Mantion, A.; Muller, A. H. E.; Pieles, U.; Taubert, A.; Meier, W. Silsesquioxane/Polyamine Nanoparticle-Templated Formation of Star- or Raspberry-like Silica Nanoparticles. *Langmuir* **2009,** *25*, 7109–7115.
40. Helmecke, O.; Hirsch, A.; Behrens, P.; Menzel, H. Influence of Polymeric Additives on Biomimetic Silica Deposition on Patterned Microstructures. *J. Colloid Interface Sci.* **2008,** *321*, 44–51.
41. Helmecke, O.; Hirsch, A.; Behrens, P.; Menzel, H. Microstructured Reaction Areas for the Deposition of Silica. *Colloid Polym. Sci.* **2008,** *286*, 225–231.
42. Helmecke, O.; Menneking, C.; Behrens, P.; Menzel, H. Influence of Shape and Surface Properties of Microstructured Reaction Areas on the Deposition of Silica. *Colloid Polym. Sci.* **2008,** *286*, 305–311.
43. Advincula, M. C.; Patel, P.; Mather, P. T.; Mattson, T.; Goldberg, A. J. Polypeptide-Catalyzed Silica for Dental Applications. *J. Biomed. Mater. Res., Part B* **2009,** *88B*, 321–331.
44. Patwardhan, S. V.; Maheshwari, R.; Mukherjee, N.; Kiick, K. L.; Clarson, S. J. Conformation and Assembly of Polypeptide Scaffolds in Templating the Synthesis of Silica: An Example of a Polylysine Macromolecular "Switch". *Biomacromolecules* **2006,** *7*, 491–497.
45. Baeuerlein, E. *Biomineralization, Progress in Biology, Molecular Biology, and Application*; Wiley-VCH Verlag GmbH & Co.: Weinheim, Germany, 2004.
46. Baeuerlein, E. *Handbook of Biomineralization, Biological Aspects and Structure Formation*; Wiley-VCH Verlag GmbH & Co.: Weinheim, Germany, 2007.
47. Hildebrand, M. Diatoms, Biomineralization Processes, and Genomics. *Chem. Rev. (Washington, DC, U. S.)* **2008,** *108*, 4855–4874.
48. Wenzl, S.; Hett, R.; Richthammer, P.; Sumper, M. Silacidins: Highly Acidic Phosphopeptides from Diatom Shells Assist in Silica Precipitation *in Vitro*. *Angew. Chem., Int. Ed.* **2008,** *47*, 1729–1732.
49. Zschornack, G. *Atomdaten Für Die Röntgenspektralanalyse*; Springer: Berlin, 1989.
50. Kelly, K. L.; Coronado, E.; Zhao, L. L.; Schatz, G. C. The Optical Properties of Metal Nanoparticles: The Influence of Size, Shape, and Dielectric Environment. *J. Phys. Chem. B* **2003,** *107*, 668–677.
51. Mock, J. J.; Barbic, M.; Smith, D. R.; Schultz, D. A.; Schultz, S. Shape Effects in Plasmon Resonance of Individual Colloidal Silver Nanoparticles. *J. Chem. Phys.* **2002,** *116*, 6755–6759.
52. Sosa, I. O.; Noguez, C.; Barrera, R. G. Optical Properties of Metal Nanoparticles with Arbitrary Shapes. *J. Phys. Chem. B* **2003,** *107*, 6269–6275.
53. Kreibig, U.; Vollmer, M., *Optical Properties of Metal Clusters*; Springer: Berlin, 1995.
54. Li, W. J.; Sun, T. Silica Artificial Opal Incorporated with Silver Nanoparticles. *Mater. Chem. Phys.* **2009,** *116*, 164–168.
55. Pan, A. L.; Yang, Z. P.; Zheng, H. G.; Liu, F. X.; Zhu, Y. C.; Su, X. B.; Ding, Z. J. Changeable Position of SPR Peak of Ag

Nanoparticles Embedded in Mesoporous SiO_2 Glass by Annealing Treatment. *Appl. Surf. Sci.* **2003,** *205*, 323–328.
56. Benesi, H. A.; Jones, A. C. An Infrared Study of the Water−Silica Gel System. *J. Phys. Chem.* **1959,** *63*, 179–182.
57. Smith, A. L.; Angelotti, N. C. Correlation of the SiH Stretching Frequency with Molecular Structure. *Spectrochim. Acta* **1959,** *15*, 301–301.
58. Bell, R. J.; Dean, P. Atomic Vibrations in Vitreous Silica. *Faraday Discuss.* **1970,** *50*, 51–61.
59. Bell, R. J.; Bird, N. F.; Dean, P. Vibrational Spectra of Vitreous Silica Germania and Beryllium Fluoride. *J. Phys. C* **1968,** *1*, 299–303.
60. Colomban, P. Review Raman Studies of Inorganic Gels and of Their Sol-to-Gel, Gel-to-Glass and Glass-to-Ceramics Transformation. *J. Raman Spectrosc.* **1996,** *27*, 747–758.
61. Marino, I.-G.; Lottici, P. P.; Bersani, D.; Raschellà, R.; Lorenzi, A.; Montenero, A. Micro-Raman Monitoring of Solvent-Free TEOS Hydrolysis. *J. Non-Cryst. Solids* **2005,** *351*, 495–498.
62. Thompson, W. R.; Pemberton, J. E. Raman Spectroscopy of Covalently Bonded Alkylsilane Layers on Thin Silica Films Immobilized on Silver Substrates. *Anal. Chem.* **2002,** *66*, 3362–3370.
63. Cathcart, N.; Mistry, P.; Makra, C.; Pietrobon, B.; Coombs, N.; Jelokhani-Niaraki, M.; Kitaev, V. Chiral Thiol-Stabilized Silver Nanoclusters with Well-Resolved Optical Transitions Synthesized by a Facile Etching Procedure in Aqueous Solutions. *Langmuir* **2009,** *25*, 5840–5846.
64. Nishida, N.; Yao, H.; Kimura, K. Chiral Functionalization of Optically Inactive Monolayer-Protected Silver Nanoclusters by Chiral Ligand-Exchange Reactions. *Langmuir* **2008,** *24*, 2759–2766.
65. Nishida, N.; Yao, H.; Ueda, T.; Sasaki, A.; Kimura, K. Synthesis and Chiroptical Study of D/L-Penicillamine-Capped Silver Nanoclusters. *Chem. Mater.* **2007,** *19*, 2831–2841.
66. Govorov, A. O.; Fan, Z. Y.; Hernandez, P.; Slocik, J. M.; Naik, R. R. Theory of Circular Dichroism of Nanomaterials Comprising Chiral Molecules and Nanocrystals: Plasmon Enhancement, Dipole Interactions, and Dielectric Effects. *Nano Lett.* **2010,** *10*, 1374–1382.
67. Li, T.; Park, H. G.; Lee, H.-S.; Choi, S.-H. Circular Dichroism Study of Chiral Biomolecules Conjugated with Silver Nanoparticles. *Nanotechnology* **2004,** S660.
68. Chen, W.; Oh, S.; Ong, A. P.; Oh, N.; Liu, Y.; Courtney, H. S.; Appleford, M.; Ong, J. L. Antibacterial and Osteogenic Properties of Silver-Containing Hydroxyapatite Coatings Produced Using a Sol Gel Process. *J. Biomed. Mater. Res. A* **2007,** *82*, 899–906.
69. Pal, S.; Tak, Y. K.; Song, J. M. Does the Antibacterial Activity of Silver Nanoparticles Depend on the Shape of the Nanoparticle? A Study of the Gram-Negative Bacterium *Escherichia coli*. *Appl. Environ. Microbiol.* **2007,** *73*, 1712–20.
70. Panacek, A.; Kvitek, L.; Prucek, R.; Kolar, M.; Vecerova, R.; Pizurova, N.; Sharma, V. K.; Nevecna, T.; Zboril, R. Silver Colloid Nanoparticles: Synthesis, Characterization, and Their Antibacterial Activity. *J. Phys. Chem. B* **2006,** *110*, 16248–53.
71. Sondi, I.; Salopek-Sondi, B. Silver Nanoparticles as Antimicrobial Agent: A Case Study on *E. coli* as a Model for Gram-Negative Bacteria. *J. Colloid Interface Sci.* **2004,** *275*, 177–82.
72. Kazakova, O. A.; Gun'ko, V. M.; Voronin, E. F.; Sil'chenko, S. S.; Chuiko, A. A. Interaction of Proteins with the Surface of Dispersed Silica in Aqueous Suspensions. *Colloid J.* **1998,** *60*, 563–567.
73. Gun'ko, V. M.; Mikhailova, I. V.; Zarko, V. I.; Gerashchenko, I. I.; Guzenko, N. V.; Janusz, W.; Leboda, R.; Chibowski, S. Study of Interaction of Proteins with Fumed Silica in Aqueous Suspensions by Adsorption and Photon Correlation Spectroscopy Methods. *J. Colloid Interface Sci.* **2003,** *260*, 56–69.
74. Orts-Gil, G.; Natte, K.; Drescher, D.; Bresch, H.; Mantion, A.; Kneipp, J.; Österle, W., Characterisation of Silica Nanoparticles Prior to *in Vitro* Studies: From Primary Particles to Agglomerates. *J. Nanopart. Res.* DOI: 10.1007/s11051-010-9910-9.
75. Lison, D.; Thomassen, L. C. J.; Rabolli, V.; Gonzalez, L.; Napierska, D.; Seo, J. W.; Kirsch-Volders, M.; Hoet, P.; Kirschhock, C. E. A.; Martens, J. A. Nominal and Effective Dosimetry of Silica Nanoparticles in Cytotoxicity Assays. *Toxicol. Sci.* **2008,** *104*, 155–162.
76. Kang, S. M.; Lee, K. B.; Kim, D. J.; Choi, I. S. Biomimetic Approach to the Formation of Gold Nanoparticle/Silica Core/Shell Structures and Subsequent Bioconjugation. *Nanotechnology* **2006,** *17*, 4719–4725.
77. Xu, L. M.; Wang, J. X.; Wen, L. X.; Chen, J. F. Fabrication and Characterization of Ag-SiO_2 Composite Hollow Nanospheres. *J. Mater. Sci.* **2006,** *41*, 517–523.
78. Mahltig, B.; Gutmann, E.; Reibold, M.; Meyer, D. C.; Bottcher, H. Synthesis of Ag and Ag/SiO_2 Sols by Solvothermal Method and Their Bactericidal Activity. *J. Sol−Gel Sci. Technol.* **2009,** *51*, 204–214.
79. Gautier, C.; Burgi, T. Chiral Gold Nanoparticles. *ChemPhysChem* **2009,** *10*, 483–492.
80. Noguez, C.; Garzon, I. L. Optically Active Metal Nanoparticles. *Chem. Soc. Rev.* **2009,** *38*, 757–771.
81. Sokolov, V. I. Chiral Stereochemistry of Nanoparticles. *Russ. J. Coord. Chem.* **2009,** *35*, 553–565.
82. Chakravorty, D.; Basu, S.; Mukherjee, P. K.; Saha, S. K.; Pal, B. N.; Dan, A.; Bhattacharya, S. Novel Properties of Glass-Metal Nanocomposites. *J. Non-Cryst. Solids* **2006,** *352*, 601–609.
83. Chakravorty, D.; Basu, S.; Pal, B. N.; Mukherjee, P. K.; Ghosh, B.; Chatterjee, K.; Bose, A.; Bhattacharya, S.; Banerjee, A. Synthesis of Nanocomposites Using Glasses and Mica as Templates. *Bull. Mater. Sci.* **2008,** *31*, 263–276.
84. Knopp, D.; Tang, D. P.; Niessner, R. Bioanalytical Applications of Biomolecule-Functionalized Nanometer-Sized Doped Silica Particles. *Anal. Chim. Acta* **2009,** *647*, 14–30.
85. Rameshbabu, N.; Sampath Kumar, T. S.; Prabhakar, T. G.; Sastry, V. S.; Murty, K. V.; Prasad Rao, K. Antibacterial Nanosized Silver Substituted Hydroxyapatite: Synthesis and Characterization. *J. Biomed. Mater. Res. A* **2007,** *80*, 581–591.
86. Diaz, M.; Barba, F.; Miranda, M.; Guitian, F.; Torrecillas, R.; Moya, J. S., Synthesis and Antimicrobial Activity of a Silver−Hydroxyapatite Nanocomposite. *J. Nanomater.* 2009, Doi 10.1155/2009/498505.
87. Thiel, J.; Pakstis, L.; Buzby, S.; Raffi, M.; Ni, C.; Pochan, D. J.; Shah, S. I. Antibacterial Properties of Silver-Doped Titania. *Small* **2007,** *3*, 799–803.
88. Cioni, B.; Lazzeri, A.; Gallone, G.; Levita, G. Synthesis of Bioactive Hydroxyapatite-Zirconia Toughened Composites for Bone Replacement. *Biomed. Appl. Smart Mater., Nanotechnol. Micro/Nano Eng.* **2009,** *57*, 31–36.
89. Verne, E.; Miola, M.; Vitale Brovarone, C.; Cannas, M.; Gatti, S.; Fucale, G.; Maina, G.; Masse, A.; Di Nunzio, S. Surface Silver-Doping of Biocompatible Glass To Induce Antibacterial Properties. Part I: Massive Glass. *J. Mater. Sci. Mater. Med.* **2009,** *20*, 733–40.
90. Podsiadlo, P.; Paternel, S.; Rouillard, J. M.; Zhang, Z.; Lee, J.; Lee, J. W.; Gulari, E.; Kotov, N. A. Layer-by-Layer Assembly of Nacre-like Nanostructured Composites with Antimicrobial Properties. *Langmuir* **2005,** *21*, 11915–21.
91. Jeon, H. J.; Yi, S. C.; Oh, S. G. Preparation and Antibacterial Effects of Ag-SiO_2 Thin Films by Sol−Gel Method. *Biomaterials* **2003,** *24*, 4921–4928.
92. Bartlett, P.; Ottewill, R. H. A Neutron-Scattering Study of the Structure of a Bimodal Colloidal Crystal. *J. Chem. Phys.* **1992,** *96*, 3306–3318.
93. Kotlarchyk, M.; Chen, S. H. Analysis of Small-Angle Neutron-Scattering Spectra from Polydisperse Interacting Colloids. *J. Chem. Phys.* **1983,** *79*, 2461–2469.
94. Schulz, G. V. On the Relationship between the Rate of Reaction and Composition of the Reaction Products in

Macro Pollymerisation Processes 122 Announcement on Highly Polymeric Bonds. *Z. Phys. Chem. (Muenchen, Ger.)* **1935,** *30*, 379–398.
95. Kline, S. R. Reduction and Analysis of SANS and USANS Data Using Igor Pro. *J. Appl. Crystallogr.* **2006,** *39*, 895–900.
96. Hayter, J. B. Physics of Amphiphiles—Micelles, Vesicles, and Microemulsions. Varenna on Lake Como, Villa Monastero, 19−29 July 1983; Proceedings of the International School of Physics "Enrico Fermi", course 90; Degiorgio, V., Corti, M., Eds.; North-Holland, Elsevier Science Pub. Co.: Amsterdam, New York, 1983; pp 59−93.
97. BrunnerPopela, J.; Glatter, O. Small-Angle Scattering of Interacting Particles. 1. Basic Principles of a Global Evaluation Technique. *J. Appl. Crystallogr.* **1997,** *30*, 431–442.
98. Mittelbach, R.; Glatter, O. Direct Structure Analysis of Small-Angle Scattering Data from Polydisperse Colloidal Particles. *J. Appl. Crystallogr.* **1998,** *31*, 600–608.
99. Auwerx, J. The Human Leukemia Cell Line, THP-1: A Multifacetted Model for the Study of Monocyte−Macrophage Differentiation. *Experientia* **1991,** *47*, 22–31.
100. Park, E. K.; Jung, H. S.; Yang, H. I.; Yoo, M. C.; Kim, C.; Kim, K. S. Optimized THP-1 Differentiation Is Required for the Detection of Responses to Weak Stimuli. *Inflamm. Res.* **2007,** *56*, 45–50.